Applied Thermal Engineering 111 (2017) 903–913

Contents lists available at ScienceDirect

Applied Thermal Engineering

journal homepage: www.elsevier.com/locate/apthermeng

Research Paper

An investigation of heat transfer losses in reciprocating devices

Caroline Willich [a], Christos N. Markides [b], Alexander J. White [a,*]

[a] Department of Engineering, Cambridge University, CB2 1PZ, United Kingdom
[b] Department of Chemical Engineering, Imperial College, London SW7 2AZ, United Kingdom

HIGHLIGHTS

- Computed dissipation in gas springs matches experiment over a wide speed range.
- A gas spring with internal grid has been simulated to mimic valve flow.
- Grid-generated motions roughly double the thermal loss at high Peclet number.
- Thermal loss is significant in the context of high-efficiency compressors.

ARTICLE INFO

Article history:
Received 27 July 2016
Revised 20 September 2016
Accepted 24 September 2016
Available online 28 September 2016

Keywords:
Reciprocating compression
Reciprocating expansion
Irreversible heat transfer
Gas springs
Hysteresis loss

ABSTRACT

The paper presents a detailed computational-fluid-dynamic study of the thermodynamic losses associated with heat transfer in gas springs. This forms part of an on-going investigation into high-efficiency compression and expansion devices for energy conversion applications. Axisymmetric calculations for simple gas springs with different compression ratios and using different gases are first presented, covering Peclet numbers that range from near-isothermal to near-adiabatic conditions. These show good agreement with experimental data from the literature for pressure variations, wall heat fluxes and the so-called hysteresis loss. The integrity of the results is also supported by comparison with simplified models. In order to mimic the effect of the eddying motions generated by valve flows, non-axisymmetric computations have also been carried out for a gas spring with a grid (or perforated plate) of 30% open area located within the dead space. These show significantly increased hysteresis loss at high Peclet number which may be attributed to the enhanced heat transfer associated with grid-generated motions. Finally, the implications for compressor and expander performance are discussed.

1. Introduction

Reciprocating compressors and expanders have a wide range of potential applications for energy conversion systems. Examples include reciprocating Joule cycles for combined heat and power plant [1], heat pumps [2], Stirling engines (e.g., for solar applications [3]) and free-piston engines [4]. The present study was motivated by applications in energy storage, specifically the 'pumped heat energy storage' (PHES) system described in Refs. [5,6]. One advantage of reciprocating devices for such purposes is that, relative to turbomachinery, they offer the potential for high compression and expansion efficiency. This is especially true for low-power systems for which turbomachines suffer high leakage and windage loss. Furthermore, a single device may serve as both a compressor and expander by adjustment of valve timings. This is beneficial for energy storage applications as it reduces the cost and turn-round time between charge and discharge.

The potential for high efficiency of reciprocating devices is rooted in the near-reversible behaviour of gas systems when subjected to pure displacement work, at least in the isothermal and adiabatic limits. For real machines, several irreversible processes nonetheless occur, including throttling through valves, mixing of inlet and residual gas, and leakage past piston rings. Various mechanical losses also occur due to friction in bearings, valve gear and piston rings. Methods of mitigating against these are discussed in Refs. [1,5] and include reducing piston speed and maximising valve open areas. However, once these losses have been minimised the effects of heat transfer are likely to remain a major factor limiting efficiency. In this respect it is important to note that, even if the device is insulated such that processes are globally adiabatic, heat exchange to and from the cylinder walls (but with no *net* heat transfer) is inherently irreversible and incurs an exergetic loss. The main purpose of the present paper is to investigate this loss using

* Corresponding author.
E-mail address: ajw36@cam.ac.uk (A.J. White).

http://dx.doi.org/10.1016/j.applthermaleng.2016.09.136
1359-4311/

CFD analysis, the ultimate aim being to determine what impact it has on compression and expansion efficiency and what steps can be taken to reduce it.

1.1. Previous work

In the 1960s Annand [7] reviewed published experimental work on heat transfer in IC engines, concluding that the use of traditional heat transfer coefficients (HTCs) was not suitable because the heat flux and driving temperature difference are not in phase. A simple 1-D heat conduction analysis by Pfriem [8], using small amplitude pressure fluctuations to model work transfer, had however already established that unsteady effects could be modelled with a *complex* HTC. Later work by Lawton [9] replaced the pressure fluctuations with volume fluctuations, these being better defined and independent of the machine speed.

Much of the current understanding of heat transfer irreversibility in reciprocating devices stems from research on valveless gas springs. Examples include the analysis of 'hysteresis loss' by Lee [10] using an approach similar to that of Pfriem, and the detailed loss measurements conducted by Kornhauser and co-workers (e.g., [11]) which generally agree well with Lee's theory. More recently, Bailey et al. [12] undertook similar experiments but with clearance (rather than 'sliding') seals, concluding that Lee's analysis remained valid provided account is taken of the pumping loss. Other recent work includes the conjugate heat transfer analysis by Mathie et al. [13] which shows that finite conductivity of the cylinder wall is an important factor for some combinations of gas and wall properties.

Detailed computational studies include the axisymmetric calculations devised by Catto and Prata [14] and the commercial CFD simulations of Lekic and Kok [15], both applied to gas springs. The former showed excellent agreement with Lawton's model for instantaneous heat flux, but agreement with the complex HTC model was less good. Lekic and Kok obtained good agreement between predicted heat fluxes and those derived from p–V measurements, as described further in Section 4.4. They also showed the presence of secondary flows near top and bottom dead centre, highlighting that flow patterns are quite complex even in the case of simple gas springs – i.e., without valve flows.

The specific contributions of the present paper are to validate CFD analysis (particularly its ability to predict hysteresis loss in gas springs) over the full range of speed from near-isothermal to near-adiabatic, and then to provide a preliminary study into the effects of grid-generated motions in order to mimic valve flows. The role of the above-mentioned secondary flows is also considered. Simplified models for property variations are presented alongside the CFD results, partly to ensure integrity of the numerical methods, but also as an aid to physical interpretation and as a check on the assumptions involved in deducing heat fluxes from experimental p–V data. We begin with a description of the hysteresis loss in gas springs and how this can be interpreted as an efficiency decrement.

Notation

A	piston area, m^2
A_s	internal surface area, m^2
c_p	isobaric specific heat capacity, $J\,kg^{-1}\,K^{-1}$
D	piston diameter, m
D_h	hydraulic mean diameter, $4V/\overline{A}_s$, m
ℓ	connecting rod length, m
k	thermal conductivity of gas, $W\,m^{-1}\,K^{-1}$
M	mass of gas, kg
p	gas pressure, Pa
Pe	Peclet number, see Eq. (1)
$\dot{Q}$	heat transfer rate *into* gas, W
$\dot{q}_w$	wall-to-gas heat flux, $W\,m^{-2}$
R	gas constant, $J\,kg^{-1}\,K^{-1}$
r_c	crank throw, m
r_v	volumetric compression ratio ($= V_{max}/V_{min}$)
s	stroke length ($= 2r_c$), m
T_b	bulk (mass-averaged) gas temperature, K
T_w	wall temperature, K
V	gas volume, m^3
$\dot{W}$	rate of work done *by* the gas, W
x	axial location in cylinder m
X	instantaneous piston position m
α	thermal diffusivity ($= k/\rho c_p$) $m^2\,s^{-1}$
γ	ratio of specific heats
ζ	dimensionless loss, see Eq. (2)
ψ	efficiency decrement, see Eq. (4)
θ	crank angle, °
ω	anglar velocity, $rad\,s^{-1}$

Other symbols are defined in the text close to where they are used.

2. Thermal hysteresis in gas springs

A gas spring comprises a fixed mass of gas enclosed within a valveless cylinder-piston arrangement, as shown in Fig. 1. Applications include shock absorbers, hydraulic accumulators and free-piston Stirling engines, but gas springs also provide useful facilities for studying heat transfer effects. As shown the piston is driven by a motor so as to provide periodic compression and expansion which, after an initial transient, reaches a steady cyclic state. Due to the large thermal inertia, the cylinder and piston walls maintain an approximately constant and uniform temperature T_w, whereas the gas temperature adapts during the transient phase such that its minimum and maximum values straddle T_w. Thus, near top dead centre (TDC), when the gas is at its hottest, heat transfer tends to be from the gas to the walls (i.e., negative heat transfer), whereas it is in the opposite sense near bottom dead centre (BDC). As noted above, heat exchange cannot be modelled accurately using a traditional HTC because interaction between heat and work exchange result in the heat flux being out of phase with the temperature difference $\Delta T = T_w - T_b$, where T_b is the mass-averaged (or 'bulk') gas temperature.

The impact of gas-wall heat exchange depends largely on the rapidity of the compression-expansion process relative to the rate of heat transfer. This is quantified dimensionlessly by the Peclet number, Pe, which is proportional to the ratio between the thermal diffusion time and the rotational period,

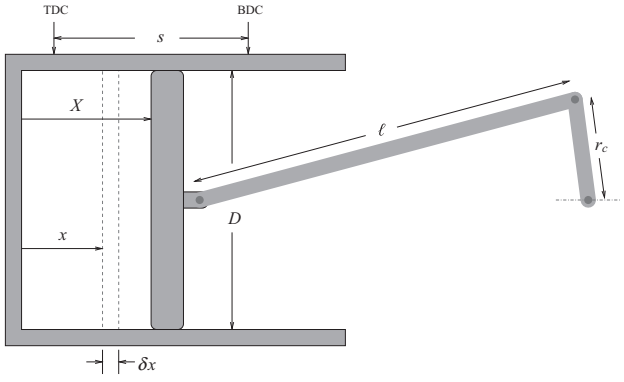

Fig. 1. Schematic of gas spring showing control volume (dashed line) used in the analysis of Section 4.2 and dimension definitions.

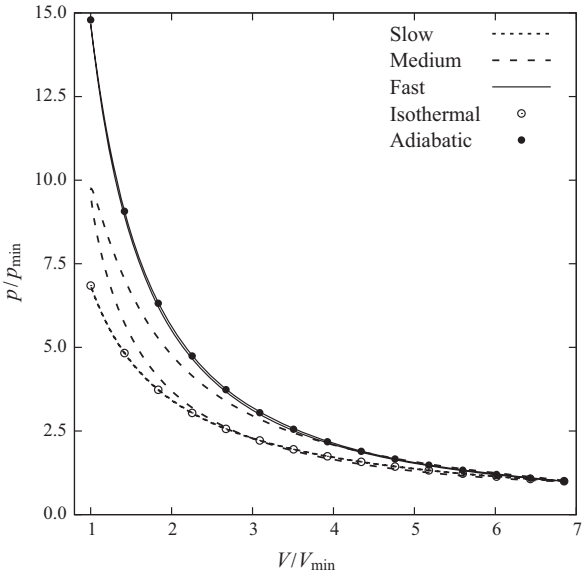

Fig. 2. Computed p–V curves at different rotational speeds for a compression ratio of $r_v = 6.8$. Slow, medium and fast correspond to Peclet numbers of ∼0.06, ∼11 and ∼8500 respectively. Isothermal and adiabatic (isentropic) relations, $pV = \text{const.}$ and $pV^\gamma = \text{const.}$ respectively, are also shown.

$$Pe = \frac{\omega D_h^2}{4\alpha} \tag{1}$$

where α is the thermal diffusivity of the gas. For very slow and very fast rotations, compression and expansion occur almost reversibly since the processes then approach the isothermal and adiabatic limits respectively. This is shown in Fig. 2 where p–V curves (generated using the CFD method described in Section 3) are almost exactly retraced for the forward and backward piston strokes at both low and high speed (Peclet numbers of ∼0.06 and ∼8500 respectively), and closely match the corresponding isothermal and isentropic relations. However, for intermediate speeds (e.g., $Pe \sim 11$) the compression and expansion curves become distinct resulting in a net work input to (and heat loss from) the gas during each cycle. This 'lost work' constitutes the hysteresis loss and is due almost entirely to thermal dissipation, as may be shown by repeating the CFD simulation at the same speed but with adiabatic wall conditions, whence the isentropic p–V curve is recovered.

2.1. Loss coefficients

The hysteresis loss has been the subject of several theoretical and experimental studies. Of particular note are the extensive measurements of Kornhauser and Smith [16] who showed that results for different geometries, gases and compression ratios (defined by $r_v = V_{max}/V_{min}$) almost collapse onto a single curve when plotted against Peclet number, provided the loss is expressed in the dimensionless form

$$\zeta = \frac{\oint pdV}{p_0 V_0 (p_a/p_0)^2 (\gamma - 1)/\gamma} \tag{2}$$

where $p_0 = (p_{max} + p_{min})/2$ and $p_a = (p_{max} - p_0)$. The normalisation in this expression stems from the analysis due to Lee [10] which results in the theoretical relation for ζ,

$$\zeta = \frac{\pi}{2y} \frac{\cosh y \sinh y - \sin y \cos y}{\cosh^2 y - \sin^2 y} \tag{3}$$

where $y = (Pe/8)^{1/2}$. Despite the scientific appeal of representing all results with a single curve, the coefficient ζ does not give an intuitive feel for how hysteresis loss affects efficiency. Furthermore, Lee's analysis is based on a linear model and thus would not be expected to apply at high compression ratios, as indeed was observed experimentally. In addition to Eq. (2) we therefore define an efficiency decrement which is obtained by attributing half the loss to compression and half to expansion and normalising by the magnitude of the actual work transfers during these processes. Thus,

$$\psi = 1 - \eta = \frac{\oint pdV}{\oint |pdV|} \tag{4}$$

where η corresponds to a compression or expansion efficiency.

3. Computational methods

Simulations were performed using the coldEngineFoam solver of OpenFOAM, version 2.3.0 [17]. This is a transient flow solver for which the underlying numerical scheme is based on a combination of the PISO (Pressure Implicit with Splitting of Operator) and SIMPLE (Semi-Implicit Method for Pressure Linked Equations). These are variants of the pressure correction method developed by Patankar and Spalding (see [18]) for incompressible flows. (The flow is incompressible in the sense that Mach numbers are very low, peak values being around 0.06, whereas flow-induced density variations are only significant for $M \gtrsim 0.3$. OpenFOAM compressible flow solvers have also been applied to reciprocating compression [19].) The model used here assumes perfect gas behaviour ($p = \rho RT$ and constant c_p) and constant dynamic viscosity and Prandtl number based on average values over the temperature ranges of interest. The RAS (Reynolds-averaged simulation) $k - \epsilon$ model is used to model turbulence, which is deemed suitable for flows with small pressure gradients and no flow separation [20], and is less computationally costly than other models [21].

3.1. Geometric details

Two different gas spring geometries were studied: the first corresponds to the lowest compression ratio experiments ($r_v = 2$) of Kornhauser and Smith (see [22]) and the second is for a higher compression ratio facility ($r_v = 6.8$) currently under development and described by Mathie et al. [23]. This higher value of r_v is more representative of the compression and expansion devices that would be used in a PHES system. Unsteady pressure and volume data are available for the first (but not yet for the second) geometry from which heat transfer rates may be inferred on the basis of a few assumptions, as described in Section 4.4. Geometric details for the two cases are presented in Table 1, and calculations were undertaken at rotational speeds ranging from 0.01 to 16 000 RPM with helium as the working fluid for geometry 1 and helium or air for geometry 2. Except where otherwise stated, isothermal wall conditions were applied on all solid boundaries, with $T_w = 300$ K.

3.2. Computational mesh and mesh dependence

For simple gas springs (i.e., without grids) the problem is essentially axisymmetric and it is sufficient to simulate a small slice (5°) from the cylinder, as shown in Fig. 3 In all cases the mesh moves with the piston so as to maintain the same number of mesh cells within the computational domain with the same relative axial spacing throughout the cycle. The meshes are also stretched so as to provide better resolution near the walls.

In order to examine the effects of mesh dependence, axisymmetric calculations were undertaken for geometry 2 at 1500 RPM using four different meshes. The coarsest mesh (mesh 1) contains 40 axial and 40 radial cells, and between each of the subsequent meshes the number of cells in each direction is doubled. Computed

Table 1
Geometric details of the two gas springs and ratios between Peclet numbers and RPM.

Geometry	Bore	Stroke	Clearance	Con. rod	Vol. ratio	Pe: RPM	
	D (mm)	s (mm)	X_{TDC} (mm)	ℓ (mm)	r_v (mm)	Air	He
1 [22]	50.8	76.2	76.2	183	2.00	N/A	0.34
2 [23]	105	78.0	13.5	150	6.77	5.65	0.69

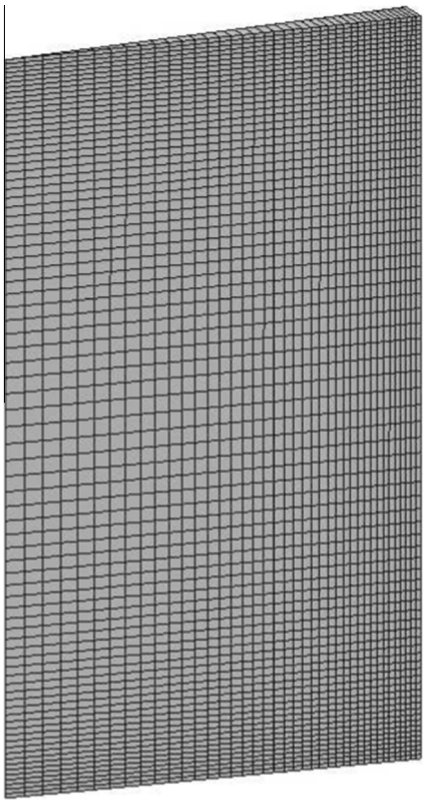

Fig. 3. Coarsest computational mesh for simple gas spring.

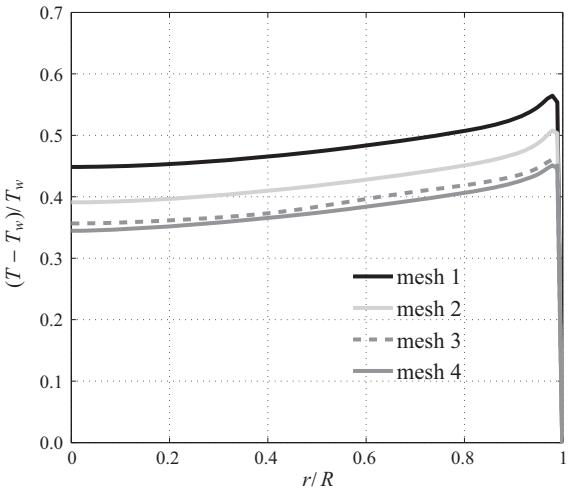

Fig. 4. Radial temperature profiles for the four different meshes. Geometry 2, at 1500 RPM with air.

radial temperature profiles 6 mm below the cylinder head are shown in Fig. 4. Local temperature differences between meshes 3 and 4 are less than 1% and the mass-averaged temperature differs by less than 1 K over the whole cycle. Mesh 3 was therefore used for the majority of simulations, but it should be noted that lower speed cases are better resolved due to the thicker boundary layers. Choosing a coarser mesh resulted in modest differences in the heat transfer phase shift at high RPM.

4. Results and discussion

Despite the simple geometry, the physical processes that occur within gas springs are quite complex due to interactions between heat and work transfer. As with all CFD simulations, it is therefore important to carry out some initial checks to ensure correct implementation of boundary conditions and the integrity of the underlying numerical scheme. This has been achieved here by comparison of results with simplified models and with experimental data where available. Thus validated, the CFD simulations are then applied in a speculative manner to examine the effects of grid-generated eddying motions.

4.1. Comparison with 1D model

The isothermal and adiabatic relations plotted in Fig. 2 constitute a 'zero-dimensional' model (i.e., uniform properties throughout) and the good agreement obtained for these limiting cases already lends some confidence to the numerical scheme. However, it is also useful to consider a simplified 1D model (as described by [9]) for the purposes of both validation and to examine the extent of pressure non-uniformities (the latter being important for interpreting p–V measurements). In this model, density is assumed uniform ($\rho = M/V$) but pressure and velocity vary with x and all properties vary with time. Mass continuity thus gives

$$\frac{\partial u}{\partial x} = -\frac{1}{\rho}\frac{\partial \rho}{\partial t} = \frac{\dot{X}}{X} \tag{5}$$

where the right-hand equality is obtained by noting M is constant and $V = AX$. Eq. (5) implies the intuitive result that the gas velocity varies linearly from zero at the cylinder head to the piston velocity $\dot{X}$ at $x = X$ (see Fig. 1 for notation). Applying the inviscid momentum equation then gives

$$\frac{\partial p}{\partial x} = -\rho\left(\frac{\partial u}{\partial t} + u\frac{\partial u}{\partial x}\right) = -\frac{Mx\ddot{X}}{AX^2} \tag{6}$$

which yields a quadratic variation for $p(x)$. Integrating between $x = 0$ and $x = X$ gives the cylinder-head-to-piston pressure difference,

$$\Delta p = p(0) - p(X) = \frac{M\ddot{X}}{2A} \tag{7}$$

which is the maximum pressure non-uniformity expected throughout the cylinder. Examples of computed axial velocity distributions and Δp are compared with the 1D model in Fig. 5. Velocities predicted by the CFD are not quite linear in x, which may be attributable to minor density variations and the impact of the side-wall boundary layer, but pressure variations agree well with the simple theory. Based on Eq. (7), the maximum pressure non-uniformity as a fraction of the instantaneous average pressure, $\Delta p/p$, will occur at

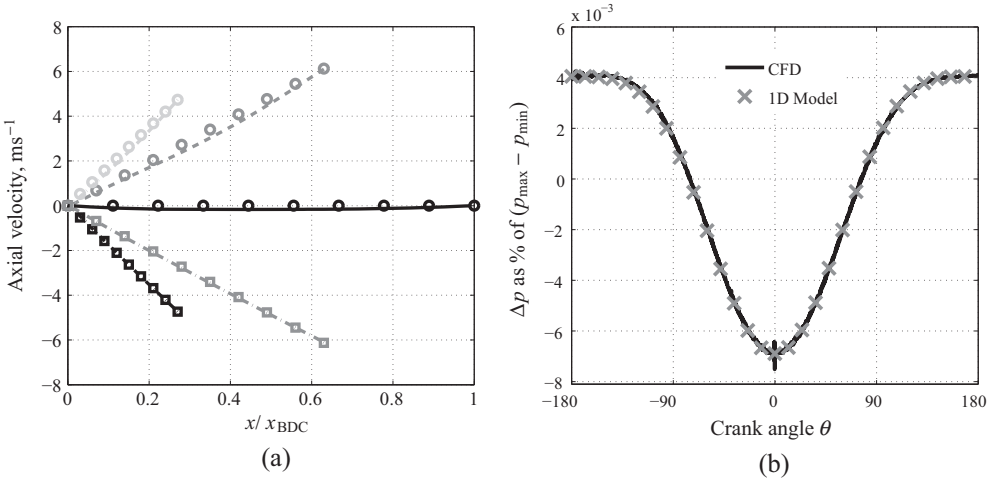

Fig. 5. Comparison with 1D model: (a) axial velocity profiles at different crank angles and (b) axial pressure difference Δp *versus* crank angle. Results are for geometry 2 at 1500 RPM with air. Lines are CFD, symbols are the 1D model.

BDC and in the worst case (for geometry 2 at 1500 RPM) is only ~0.1%.

4.2. Comparison with measured hysteresis loss

Simulations were carried out for geometry 1 at speeds of 0.01–1500 RPM with helium as the working fluid. The dimensionless loss coefficients (ζ in Eq. 2) are compared with the measurements of Kornhauser and Smith [16] in Fig. 6a. The trends are very well reproduced, although predicted losses are generally slightly lower than the measurements. For comparison, computed values of ζ for geometry 2 ($r_v = 6.8$) are also shown, using both air and helium as the working fluid. The results do not quite collapse onto a single curve with noticeable discrepancies between the different compression ratios, particularly at low speed. (By contrast, measurements at $r_v = 8$ reported in Ref. [16] showed divergence from the $r_v = 2$ case only at high speed. It is quite likely, however, that this was a consequence of the long 'appendix gap' between the cylinder and piston in the experimental set up, within which the temperature would be expected to approach T_w. This matter is discussed further in Kornhauser and Smith's paper.)

The computed losses are replotted in Fig. 6b as efficiency decrements, as defined by Eq. (4). In this format they emphasise the effect of the volume ratio and the type of gas (in particular, its heat capacity ratio, γ). A qualitative explanation for the differences lies in the higher temperature swing ($T_{max} - T_{min}$) that occurs with increasing r_v and increasing γ. This in turn leads to higher instantaneous gas-wall temperature differences ΔT. Since thermal dissipation rate scales approximately as ΔT^2, the lost work increases more rapidly than the actual work, thereby decreasing the efficiency. Note that Fig. 6b also shows results for simulations with adiabatic wall conditions for which predicted losses are negligible, confirming that thermal dissipation is the dominating factor.

4.3. Temperature variations

Except in the isothermal limit, the mass-averaged temperature T_b within the cylinder (and hence the internal energy U) varies periodically over each cycle. Typical variations of T_b for the first 15 cycles of computation are shown in Fig. 7a for both isothermal and adiabatic wall conditions. These simulations were started with uniform gas temperature at BDC equal to T_w in order to emphasise the initial transient. For the isothermal wall condition the mean temperature thus falls for the first few cycles, reaching a periodic steady state after about 20 cycles. By contrast, T_b rises very slightly from one cycle to the next for the adiabatic case and in theory no steady state is achieved due to the small entropy rise associated with viscous dissipation.

Variations of T_b over a single cycle are compared for different speeds in Fig. 7b. Near the adiabatic limit (i.e., at 1500 RPM) minimum and maximum temperatures coincide with BDC and TDC respectively, but at lower speeds these extremes occur earlier. This may be explained by straightforward application of the First Law applied to the gas system,

$$\frac{dU}{dt} = \dot{Q} - \dot{W} = \dot{Q} - p\frac{dV}{dt} \tag{8}$$

When heat transfer rates are negligible relative to work transfer (i.e., at high speed) the turning points for U necessarily coincide with those for V, but as $\dot{Q}$ becomes an increasing fraction of $\dot{W}$ (i.e., as the isothermal limit is approached) the maximum and minimum of U (and thus of T_b) must occur before the minimum and maximum volumes respectively. As $Pe \to 0$, the figure shows that T_{min} and T_{max} occur at approximately $\pm 45^\circ$ relative to TDC. (Simple 'zero-dimensional' theory based on a complex Nusselt number approach – not included here due to space constraints – is able to reproduce this result and also shows that the phase shift depends on r_v.)

In contrast to the near-uniform pressure field, significant spatial variations occur for the gas temperature due to the formation of thermal boundary layers. Fig. 8 shows the evolution of radial temperature profiles for geometry 2 at a range of speeds. With increasing speed the effects of heat transfer are confined to progressively thinner boundary layers, and the difference between the profiles during compression and expansion (e.g., at $\pm 40^\circ$) become less significant. This reflects the fact that temporal variations in p, T and $1/V$ are all aligned in the adiabatic limit.

Fig. 8 also helps explain how the gas-wall heat transfer can be out of phase with the mean temperature difference. Focussing on the 60 RPM case, the centreline temperature is near its lowest value at $\theta = -180^\circ$ (BDC) and the gradient near the wall is then such that heat flows into the gas. At $\theta = -80^\circ$ the centreline temperature has risen due to the compression work, but at a point part way through the thermal boundary layer the temperature has increased by approximately the same factor. The wall temperature is fixed so this results in a maximum within the radial profile, such that the heat flux is now towards the wall and in the opposite direction to that implied by the (bulk) gas-wall temperature

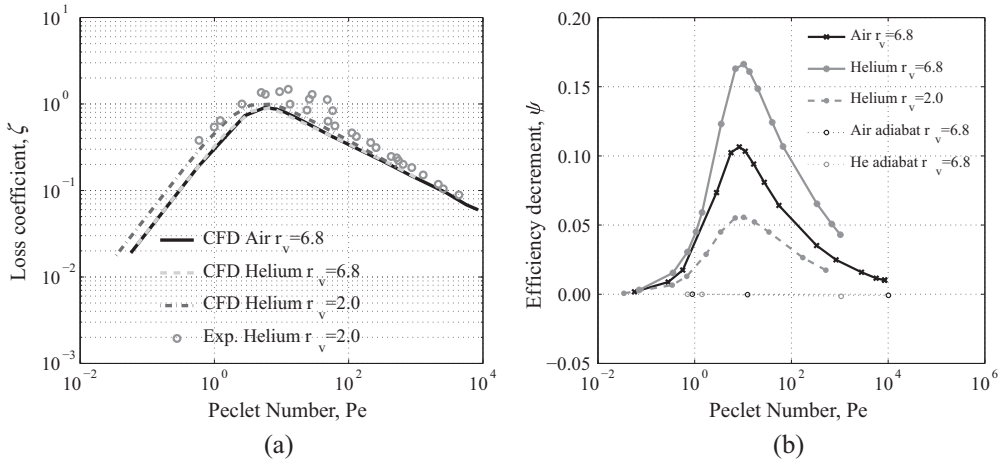

Fig. 6. Hysteresis loss: (a) expressed as a dimensionless loss coefficient ζ (Eq. (2)) compared with the experiments from Ref. [16] and (b) expressed as an efficiency decrement ψ (Eq. (4)).

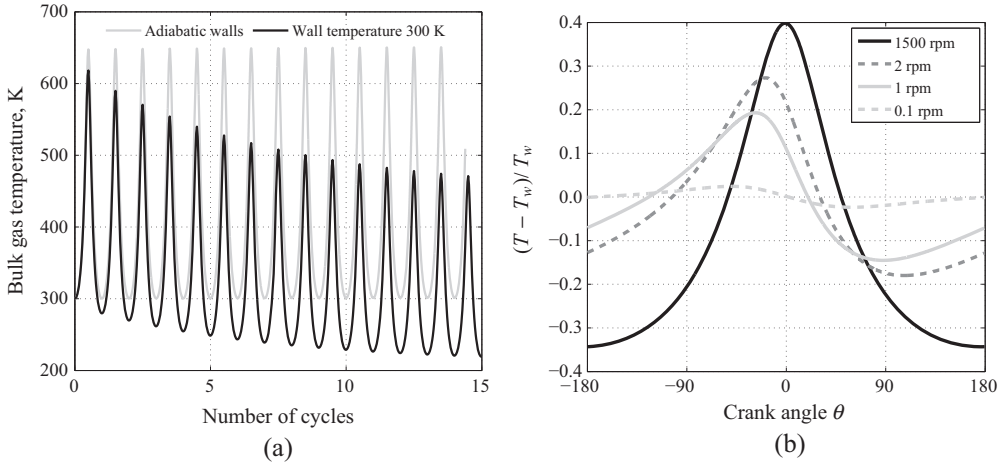

Fig. 7. Mass-averaged temperature (a) over first 15 cycles for 1500 RPM and (b) *versus* crank angle for different piston speeds at steady state. Results are for geometry 2 with air as the working fluid. Conversion between RPM and *Pe* is given in Table 1.

difference. Later through the cycle the profile is again monotonically increasing from the wall to the centreline and the expected direction of heat flux based on ΔT is restored. This sequence of events is in accord with the qualitative description given by Lawton [9].

4.4. Pressure variations and wall heat fluxes

As discussed by Kornhauser and Smith [22], experimental pressure-volume data can be used to infer instantaneous gas-wall heat transfer rates provided (i) the pressure is uniform throughout the cylinder (see discussion in Section 4.1) and (ii) perfect gas relations apply (including constant c_p), as is the case for inert gases in the temperature range considered. The First Law may therefore be written in the form,

$$\dot{Q} = \frac{d}{dt}\left(\frac{pV}{\gamma - 1}\right) + p\frac{dV}{dt} \tag{9}$$

Fig. 9 shows an example of computed pressure variations with crank angle and the corresponding heat fluxes obtained using Eq. (9). Results are compared with experimental data presented by Lekic and Kok [15] using the same experimental apparatus as that in Ref. [22]. Agreement between the predicted and "measured" heat fluxes is reasonable and although the accuracy of the computed results will be limited by the turbulence model and other modelling assumptions (e.g., uniform wall temperature and constant transport properties), it is also likely that the experimental results are affected by the clearance gap issue, as discussed in Section 4.2. Heat fluxes computed directly from

$$\dot{q}_w = -k\left.\frac{\partial T}{\partial n}\right|_w \tag{10}$$

and averaged over all surfaces are also shown in Fig. 9b. Agreement with the flux derived from Eq. (9) is very good and provides a further consistency check on the OpenFOAM calculations, confirming that energy is globally conserved.[1]

It is also of interest to examine how computed heat fluxes vary between the different internal surfaces and so Eq. (10) has been applied to obtain surface-averaged fluxes for the cylinder head, piston face and cylinder liner respectively. Results are shown in Fig. 10 for geometry 2 at speeds of 2 RPM and 1500 RPM. In both cases the three fluxes are approximately equal over much of the cycle, but significant differences emerge near TDC. It is also notable

[1] The "wallHeatFlux" post-processing utility available with OpenFOAM did not however yield a consistent result with 1st Law analysis. Values of q_w shown in the figure were obtained by implementing Eq. (10) directly within the solver.

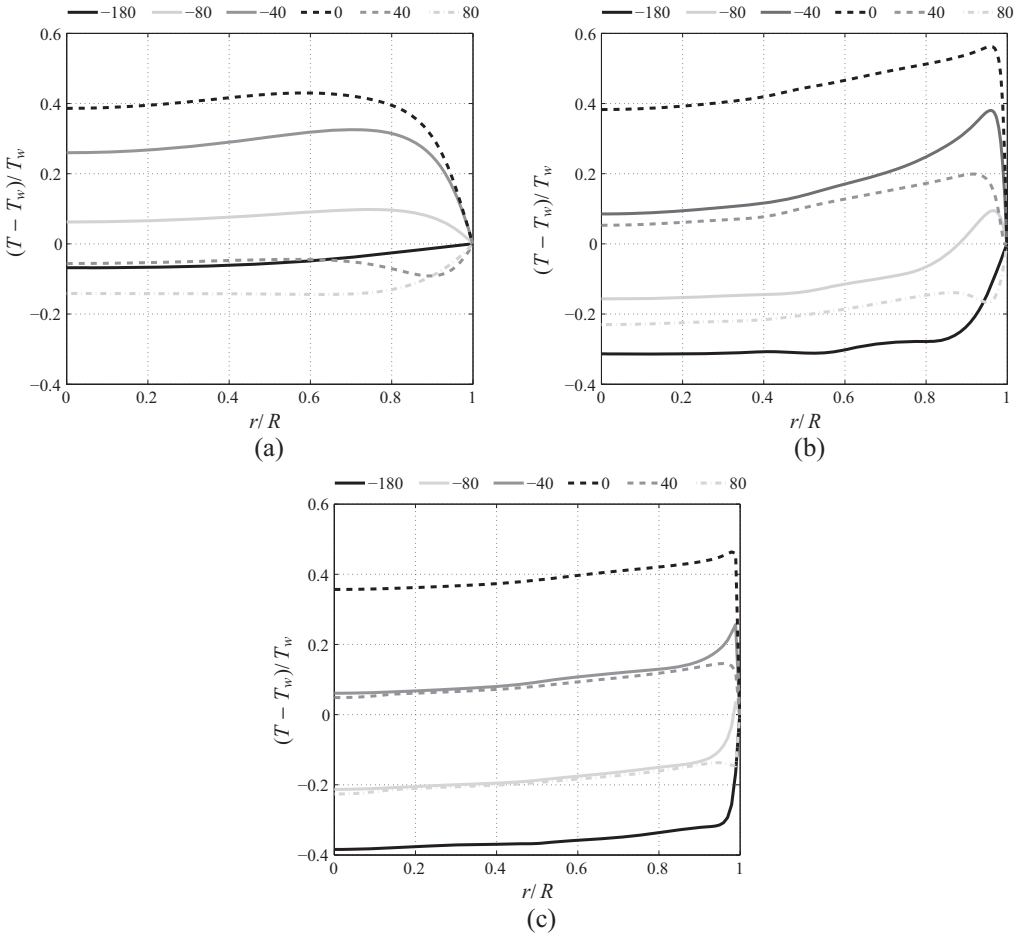

Fig. 8. Radial temperature profiles at (a) 2 RPM, (b) 60 RPM and (c) 1500 RPM. Results are for geometry 2 with air as the working fluid.

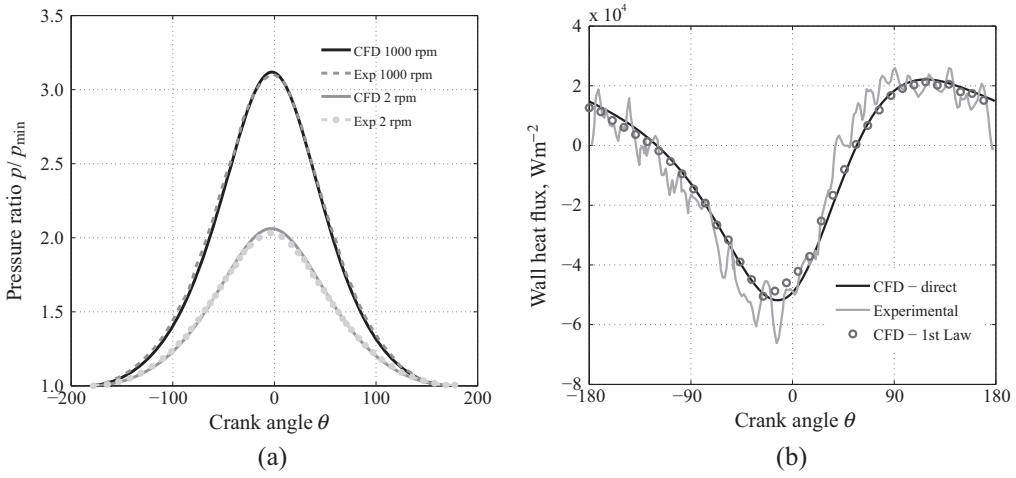

Fig. 9. (a) Pressure ratio *versus* crank angle for two different piston speeds and (b) Wall heat flux for 2 RPM. CFD simulations and experimental data taken from [15]. Results are for geometry 1 with helium.

that the trends are different for low and high speed with heat losses being highest at the cylinder head for the former and at the piston face for the latter. These differences are tied to the strong secondary flow features that occur near TDC, as reported in Ref. [15] and shown in Fig. 11. At 2 RPM (Fig. 11a) a clockwise-rotating vortex is formed that has the effect of convecting hot fluid from the middle of the flow onto the top (cylinder-head) surface, thereby enhancing heat losses relative to those on the liner and piston face. At 1500 RPM the situation is more complex, but it is notable that the main vortical structure is in the opposite (counter-clockwise) direction. Calculations undertaken with adiabatic wall conditions (and hence resulting in uniform temperature and density) revert to a clockwise vortex for this high speed case (see Fig. 11d) and thus suggest that the

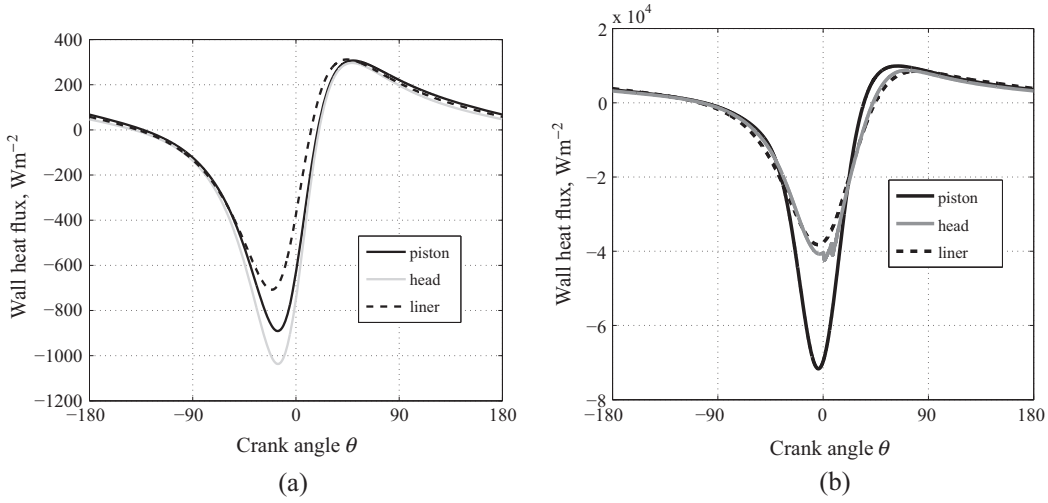

Fig. 10. Wall heat fluxes computed from Eq. (10) at (a) 2 RPM and (b) 1500 RPM. Results are for geometry 2 with air.

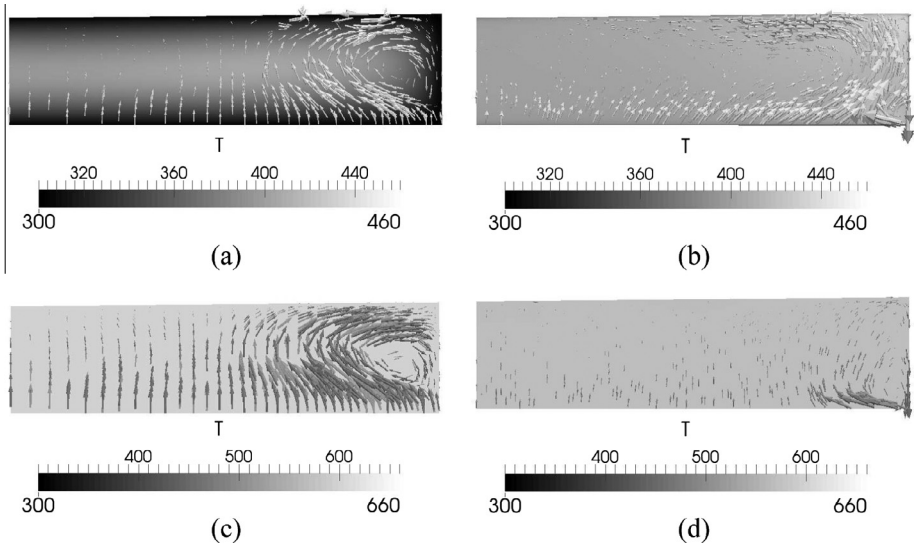

Fig. 11. Contours of temperature and velocity vectors. (a) 2 RPM, (b) 1500 RPM, (c) 2 RPM adiabatic and (d) 1500 RPM adiabatic. Results are for geometry 2 with air. Note that temperatures are uniform for the adiabatic cases and nearly uniform for the high speed case due to the very thin boundary layer.

change in the sense of rotation stems from the strong density gradients near to the wall. Note that some experimental evidence for these types of vortical structure is provided by the study of flow in a moving corner conducted by Tabaczynski et al. [24].

4.5. Calculations with an internal grid

The ultimate objective of the present work is to investigate the impact of thermal effects on the performance of reciprocating compressors and expanders, and these are qualitatively different from gas springs. For example, the opening of delivery valves in compressors will probably prevent the vortical flows near TDC described above, whereas turbulence generated by the inflow is likely to enhance wall heat transfer. Similar effects are to be expected within expanders. As a first step towards modelling these effects, results are presented here for geometry 1 but with a perforated plate (henceforth referred to as a 'grid' and shown in Fig. 12) located at 65.4 mm below the cylinder head and 10.8 mm away from the piston at TDC. Note that this grid is qualitatively similar to the valve plate of low-loss valve system proposed in Ref. [5]. A quarter cylinder was modelled with the (quarter) grid having 12 holes, each 5×2.5 mm, giving an open area of 29.6%. The simulations were done with helium as the working fluid and the temperature boundary condition for the grid was set to zeroGradient (i.e., adiabatic). All other surfaces remained isothermal. The rationale for this choice is that a non-adiabatic condition on the grid would increase the heat transfer surface, thereby reducing D_h and making comparisons difficult. The addition of the grid generates eddying motions within the cylinder, as can be seen by the streamline patterns of Fig. 12.

Flow through the grid leads to a pressure drop, but the eddying motions and accompanying turbulence also affect heat transfer. Both these effects are expected to increase the hysteresis loss and endeavours are made here to distinguish the two. Firstly, Fig. 13 shows the pressure difference Δp (pressure at piston minus pressure at cylinder head) against crank angle for simulations at 10 000 RPM with and without the grid. With the grid in place the maximum and minimum Δp are much larger and occur at a different crank angle to the no-grid case. This is to be expected as Δp is now dominated by the stagnation pressure drop through

Fig. 12. Streamlines at TDC without and with grid.

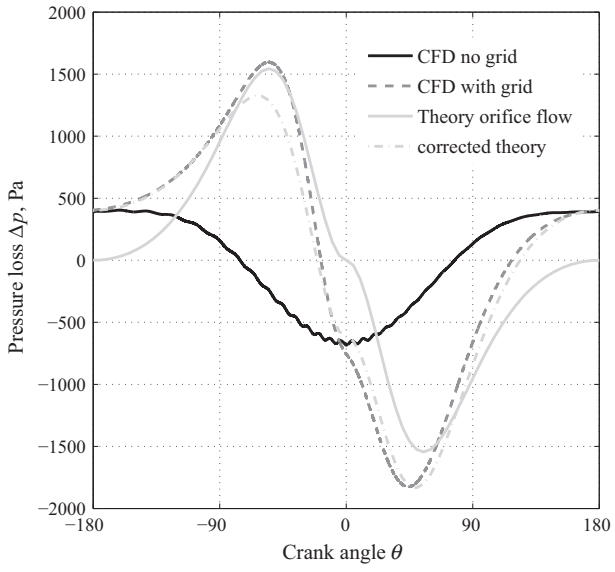

Fig. 13. Pressure drop Δp at 10 000 RPM. Geometry 1, He.

the grid which will tend to be greatest when piston speed (rather than acceleration) is greatest. An estimate of this loss may be obtained from the theory for steady flow through an orifice within a pipe,

$$\Delta p = \xi \frac{\rho}{2} v^2 \tag{11}$$

with the coefficient $\xi = 19$ for an open area of 30% (see for example [25]) and the velocity v estimated assuming the linear behaviour described in Section 4.1. As shown in Fig. 13, there is reasonably good agreement between Δp computed on this basis and that obtained from the CFD. This is further improved if the *static* pressure variation due to the piston motion (as obtained from Eq. (7)) is superimposed on the stagnation pressure loss, as shown by the curve labelled 'corrected theory'.

Fig. 14 shows average wall heat fluxes with and without the grid at different rotational speeds. The presence of the grid enhances heat transfer rates and causes a small shift towards TDC of the crank angle at which the maximum (negative) heat flux occurs. As expected, these effects are most pronounced at high speed, but they are still quite small, with the maximum heat flux increasing by just ~7% at 16 000 RPM. However, the net heat loss integrated over the cycle (which must balance the work input due to the hysteresis loss) is increased by over 70% at this speed. It should also be borne in mind that eddies generated at the grid remain quite slow due to the linear variation in axial velocity, as discussed in Section 4.1.

Finally, Fig. 15 shows the efficiency decrement calculated according to Eq. (4) with and without the grid. The effect of the grid becomes increasingly significant as the rotational speed increases, with the increased losses stemming from a combination of grid-induced pressure drop and enhanced heat transfer. These two effects may be separated out by repeating the calculations with adiabatic boundary conditions on all surfaces. The resulting losses are then due entirely to pressure drop and viscous effects and, as shown in the figure, rise with piston speed, as expected from Eq. (11). Subtracting these losses from the original (isothermal wall) results then yields an estimate of the loss component due to thermal effects alone. Despite the relatively small increase in *peak* heat flux shown in Fig. 14, the thermal loss increases by ~70% at the highest speed, in line with *net* heat loss. This is because dissipation rates (i.e., entropy generation rates) depend on the heat flux, the gas-wall temperature difference ΔT, and the relative phase of these quantities, all of which change with the grid in place.

4.6. Implications for compressors and expanders

The results of the previous section represent only a first step towards investigating the effects of valve flows. They nonetheless suggest that thermal irreversibility may be significantly increased by such flows, particularly in the near-adiabatic regime. This is precisely the regime that is of greatest interest in thermo-mechanical energy storage applications because of the reliance on near-adiabatic compression and expansion to produce the required temperature separation. As the adiabatic limit is approached, thermal losses are admittedly quite small. For example, Fig. 15 suggests a loss of around 1% at a Peclet number of about 10^4 (real machines might be expected to operate in the range $10^4 - 10^5$). However, it is worth noting that:

1. The case shown is for $r_v = 2$, corresponding to a pressure ratio of about 3.2. The loss in efficiency increases with r_v (and hence pressure ratio), as shown in Fig. 6.
2. For real valve flows, velocities at the valve plate will be a much higher fraction of the piston velocity than those at the grid in the present study, the latter being affected by the linear variation in the gas velocity.
3. Attaining a high round-trip efficiency for storage systems such as PHES relies on very high compression and expansion efficiencies, so losses of the order 1% are quite significant.

Further work is clearly required to establish the effect of other parameters (cylinder aspect ratio, grid open area, perforation size etc.), it being unlikely that Peclet number alone determines the non-dimensional loss when grids (or valves) are present.

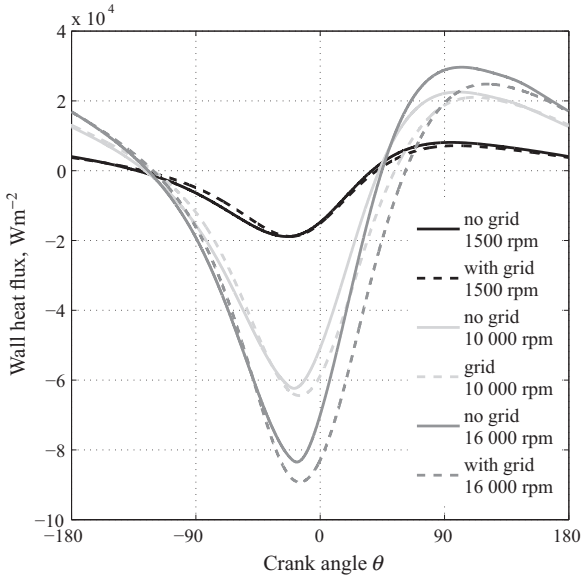

Fig. 14. Wall heat flux with and without grid for geometry 1 with He.

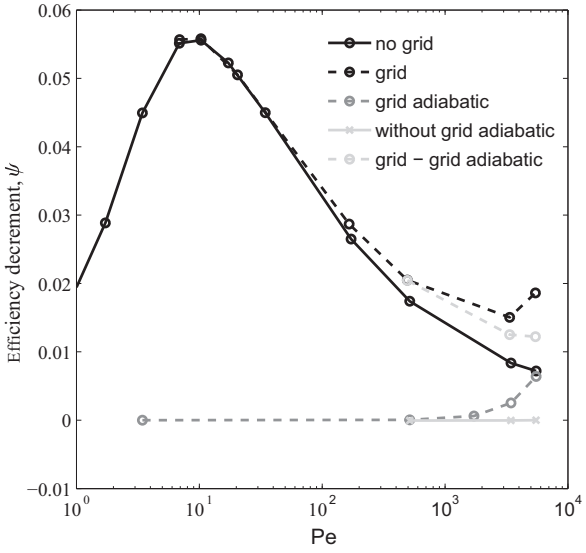

Fig. 15. Efficiency decrement ψ (Eq. (4)) *verses* Peclet number, with and without the grid. Geometry 1, He.

5. Conclusions

A computational study of gas springs has been presented, with a particular focus on heat transfer and the associated thermal dissipation. Computed values of the hysteresis loss agree well with experimental data from the literature over a wide range of Peclet numbers. Further confidence in the basic correctness of the simulations has been provided by comparison with a variety of simplified models and by self-consistency checks (e.g., by comparing average heat fluxes obtained by independent methods).

Detailed scrutiny of the results has revealed that wall heat fluxes may vary considerably over the internal surfaces (i.e., between piston face, cylinder head and cylinder liner), particularly near top and bottom dead centres. This is linked to the secondary flows that occur within the cylinder at these times and that generate significant convective effects. The structure of these flows depends on crank rotational speed, with the main vortex being predicted to change its sense of rotation at high RPM. Such effects are not accounted for in the various simplified theories of unsteady heat transfer that have been devised for gas springs and other reciprocating devices.

As a preliminary step towards investigating the impact of valve flows in reciprocating compressors and expanders, computations have also been undertaken for a gas spring containing a perforated plate (or grid) within the cylinder dead space. The resulting eddying motions are predicted to roughly double the thermal component of hysteresis loss at high Peclet numbers for the particular case considered. Although only qualitative (due to differences with real valve flows) these results suggest that thermal irreversibility may be a substantive factor limiting the efficiency of reciprocating devices, particularly in the context of the very high efficiencies sought for some energy conversion systems.

Acknowledgements

This work was supported by the UK Engineering and Physical Sciences Research Council (EPSRC), Grant EP/J006246/1. It was performed using the Darwin Supercomputer of the University of Cambridge High Performance Computing Service, provided by Dell Inc. using Strategic Research Infrastructure Funding from the Higher Education Funding Council for England and funding from the Science and Technology Facilities Council. Supporting data for the work presented in this paper are available at http://dx.doi.org/10.17863/CAM.4828.

References

[1] R.W. Moss, A.P. Roskilly, S.K. Nanda, Reciprocating Joule-cycle engine for domestic CHP systems, Appl. Energy 80 (2) (2005) 169–185, http://dx.doi.org/10.1016/j.apenergy.2004.03.007.
[2] A. White, Thermodynamic analysis of the reverse joule–brayton cycle heat pump for domestic heating, Appl. Energy 86 (11) (2009) 2443–2450.
[3] B. Kongtragool, S. Wongwises, A review of solar-powered Stirling engines and low temperature differential Stirling engines, Renew. Sustain. Energy Rev. 7 (2) (2003) 131–154, http://dx.doi.org/10.1016/S1364-0321(02)00053-9.
[4] R. Mikalsen, A. Roskilly, The design and simulation of a two-stroke free-piston compression ignition engine for electrical power generation, Appl. Therm. Eng. 28 (5) (2008) 589–600.
[5] J. Howes, Concept and development of a pumped heat electricity storage device, Proc. IEEE 100 (2) (2012) 493–503, http://dx.doi.org/10.1109/JPROC.2011.2174529.
[6] A. White, G. Parks, C.N. Markides, Thermodynamic analysis of pumped thermal electricity storage, Appl. Therm. Eng. 53 (2) (2013) 291–298, http://dx.doi.org/10.1016/j.applthermaleng.2012.03.030.
[7] W. Annand et al., Heat transfer in the cylinders of reciprocating internal combustion engines, Proc. Inst. Mech. Eng. 177 (1) (1963) 973–996.
[8] H. Pfriem, Periodic heat transfer at small pressure fluctuations, Translated from Forschung auf dem Gebiete des Ingenieurwesens, 1943.
[9] B. Lawton, Effect of compression and expansion on instantaneous heat transfer in reciprocating internal combustion engines, Proc. Inst. Mech. Eng., Part A: J. Power Energy 201 (3) (1987) 175–186.
[10] K. Lee, A simplistic model of cyclic heat transfer phenomena in closed spaces, in: Proc., Intersoc. Energy Convers. Eng. Conf., United States, 1983, p. 2.
[11] A. Kornhauser, J.L Smith Jr., Heat transfer with oscillating pressure and oscillating flow, Proceedings of the 24th Intersociety Energy Conversion Engineering Conference, 1989 (IECEC-89), vol. 5, 1989, pp. 2347–2353, http://dx.doi.org/10.1109/IECEC.1989.74802.
[12] P.B. Bailey, M.W. Dadd, J. Reed, C. Stone, T.M. Davis, Gas spring losses in linear clearance seal compressors, in: International Cryocooler Conference, 2007.
[13] R. Mathie, C.N. Markides, A.J. White, A framework for the analysis of thermal losses in reciprocating compressors and expanders, Heat Transfer Eng. 35 (16–17) (2014) 1435–1449, http://dx.doi.org/10.1080/01457632.2014.889460.
[14] A. Catto, A. Prata, A numerical study of instantaneous heat transfer during compression and expansion in piston-cylinder geometry, Numer. Heat Transfer: Part A: Appl. 38 (3) (2000) 281–303.
[15] U. Lekić, J. Kok, Heat transfer and fluid flows in gas springs, Open Thermodynam. J. 4 (2010) 13–26.
[16] A.A. Kornhauser, J.L. Smith Jr., The effects of heat transfer on gas spring performance, J. Energy Resourc. Technol. 115 (1) (1993) 70–75, http://dx.doi.org/10.1115/1.2905972.
[17] H.G. Weller, G. Tabor, H. Jasak, C. Fureby, A tensorial approach to computational continuum mechanics using object-oriented techniques, Comput. Phys. 12 (6) (1998).

[18] J.D. Anderson, J. Wendt, Computational Fluid Dynamics, vol. 206, Springer, 1995.
[19] H. Aguerre, S. Damian, J. Giminez, N. Nigro, Modeling of compressible fluid problems with openfoam using dynamic mesh technology, Mec. Comput. 32 (2013) 955–1011.
[20] J.E. Bardina, P.G. Huang, T.J. Coakley, Turbulence Modeling Validation, Testing, and Development, Tech. Rep., April 1997.
[21] I. Pantokratoras, C. Arapatsakos, Turbulence models comparison for the numerical study of the air flow, an internal combustion engine, in: Advances in Engineering Mechanics and Material, Wseas LLC, Santorini, Greece, 2014, pp. 178–184.
[22] A.A. Kornhauser, J.L. Smith Jr., Application of a complex Nusselt number to heat transfer during compression and expansion, J. Heat Transfer 116 (3) (1994) 536–542, http://dx.doi.org/10.1115/1.2910904.
[23] R. Mathie, A.J. White, C.N. Markides, Ultrasonic measurements of unsteady heat transfer in a reciprocating gas spring, in: International Conference on Heat Transfer, Fluid Mechanics and Thermodynamics, 2014.
[24] R.J. Tabaczynski, D.P. Hoult, J.C. Keck, High reynolds number flow in a moving corner, J. Fluid Mech. 42 (02) (1970) 249–255.
[25] B. Glück, Hydrodynamische und gasdynamische Rohrströmung – Druckverluste, VEB Verlag fuer Bauwesen, Berlin, 1988.